

1

2

3

4 **Maternal Obesity-Induced Endoplasmic Reticulum Stress Causes Metabolic**  
5 **Alterations and Abnormal Hypothalamic Development in the Offspring**

6

7 **Soyoung Park<sup>1</sup>, Alice Jang<sup>1</sup>, Sebastien G. Bouret<sup>1,2,\*</sup>**

8

9

10 <sup>1</sup> *The Saban Research Institute, Developmental Neuroscience Program & Diabetes and Obesity Program,*  
11 *Center for Endocrinology, Diabetes and Metabolism, Children's Hospital Los Angeles, University of*  
12 *Southern California, Los Angeles, CA 90027, USA*

13 <sup>2</sup> *Inserm, Jean-Pierre Aubert Research Center, U1172, University Lille 2, Lille, 59045, France*

14

15

16

17

18

19 **Short title:** Maternal obesity and ER stress

20

21

22

23

24

25

26 **\*Corresponding author:** Sebastien G. Bouret, Ph.D., The Saban Research Institute,  
27 Developmental Neuroscience Program & Diabetes and Obesity Program, Center for  
28 Endocrinology, Diabetes and Metabolism, Children's Hospital Los Angeles, University of  
29 Southern California, 4650 Sunset Boulevard, MS#135, Los Angeles, CA 90027, USA. Phone:  
30 +1-323-361-8743; Fax: +1-323-361-1549; E-mail: [sbouret@chla.usc.edu](mailto:sbouret@chla.usc.edu)

31 **Abstract**

32 The steady increase in the prevalence obesity and associated type II diabetes is a major health  
33 concern, particularly among children. Maternal obesity represents a risk factor that contributes  
34 to metabolic perturbations in the offspring. Endoplasmic reticulum (ER) stress has emerged as a  
35 critical mechanism involved in leptin resistance and type 2 diabetes in adult individuals. Here,  
36 we used a mouse model of maternal obesity to investigate the importance of early life ER stress  
37 in the nutritional programming of metabolic disease. Offspring of obese dams displayed  
38 increased body weight, adiposity, food intake and developed glucose intolerance. Moreover,  
39 maternal obesity disrupted the development of melanocortin circuits associated with neonatal  
40 hyperleptinemia and leptin resistance. ER stress-related genes were upregulated in the  
41 hypothalamus of neonates born to obese mothers and neonatal treatment with the ER stress-  
42 relieving drug tauroursodeoxycholic acid improved metabolic and neurodevelopmental deficits  
43 and reverses leptin resistance in neonates born to obese dams.

## 44 **Introduction**

45 A major shift in our nutritional environment has greatly contributed to the recent obesity  
46 epidemic. There is growing evidence that adverse fetal and early postnatal environments  
47 increase the risk of developing obesity. In particular, accumulative evidence from both human  
48 and animal studies demonstrated that exposure to maternal obesity predisposes offspring to  
49 develop obesity and other metabolic dysfunctions later in life [1,2,3]. The hypothalamus is  
50 involved in the control of food intake and energy expenditure and is a prime target of  
51 developmental the programming of obesity induced by maternal and perinatal nutritional  
52 imbalances [1,2,4,5,6,7]. A primary importance has been given to the arcuate nucleus of the  
53 hypothalamus (ARH) because it contains two main neuronal populations that play a major role  
54 in energy homeostasis: the anorexigenic pro-opiomelanocortin (POMC)-expressing neurons and  
55 the orexigenic neuropeptide Y (NPY) and agouti-related peptide (AgRP)-expressing neurons.  
56 The adipocyte-derived hormone leptin directly targets these neuronal populations to cause  
57 weight loss effects by stimulating POMC neurons and inhibiting AgRP/NPY neurons. Leptin also  
58 promotes the development of POMC and AgRP/NPY axonal projections during early postnatal  
59 life [8]. Prior studies have shown that maternal obesity disrupts the normal development of  
60 these neuronal circuits [9,10,11]. However, the cellular mechanisms involved in hypothalamic  
61 development and how these mechanisms are perturbed in a context of maternal obesity remain  
62 elusive.

63

64 Endoplasmic reticulum (ER) stress provides an attractive mechanism to underlie the  
65 programming effects of maternal obesity. Alterations in cellular homeostasis can lead to ER  
66 stress and the activation of the unfolded protein response (UPR) pathway. Previous studies  
67 have demonstrated that ER stress and UPR signaling pathway activation play important roles in  
68 obesity-induced insulin resistance and type 2 diabetes during adult life. Obesity caused by leptin  
69 deficiency or high-fat feeding in mice induces ER stress in peripheral tissues as well as in the

70 hypothalamus [12,13,14]. Furthermore, relieving ER stress with chemical chaperones, *i.e.*,  
71 agents that have the ability to increase ER folding machinery, increases insulin sensitivity and  
72 reverses type 2 diabetes in adult *ob/ob* mice and improves leptin sensitivity in adult obese mice  
73 fed a high-fat diet (HFD) [13,14]. Moreover, genetic manipulation of the unfolded protein  
74 response transcription factor spliced X-box binding protein (Xbp1) specifically in POMC neurons  
75 protects against diet-induced obesity and ameliorates leptin and insulin sensitivity [15]. Despite  
76 accumulative evidence supporting a role for ER stress in metabolic regulation, an association  
77 between maternal obesity, ER stress, and the programming of obesity and hypothalamic  
78 development has not yet been established.

79

80 In the present study, we investigated whether maternal diet-induced obesity induces ER stress  
81 during neonatal life in the offspring and how it contributes to the nutritional programming of  
82 obesity and hypothalamic development. We found that maternal obesity causes metabolic and  
83 neurodevelopmental alterations in the offspring accompanied with elevated ER stress in the  
84 hypothalamus and pancreas during postnatal development. Moreover, we report that  
85 pharmacological inhibition of ER stress has long-term beneficial effects on body weight, body  
86 composition, energy balance, glucose homeostasis, leptin sensitivity, and POMC axonal  
87 projections in the offspring born to obese dams. Finally, our study reveals that the  
88 neurodevelopmental effects of maternal obesity likely involve direct inhibitory action of saturated  
89 fatty acids on arcuate axon growth.

## 90 **Results**

### 91 **Maternal obesity causes metabolic disturbances in the offspring**

92 A mouse model of maternal obesity induced by high-fat high-sucrose (HFHS) feeding during  
93 pregnancy and lactation was used to study the effects of maternal obesity on the offspring's  
94 metabolism and development. Adult female mice were either fed a HFHS (58% kcal fat w/  
95 sucrose) or a control diet (6% calories from fat) six weeks before breeding. Dams were kept on  
96 their respective diet throughout pregnancy and lactation. A significant increase in dams' weight  
97 gain was observed as early as 4 weeks after HFHS diet began and persisted throughout the  
98 HFHS exposure (**Fig 1A**). This elevated body weight was associated with increased fat mass  
99 (**Fig 1B**). Moreover, dams fed a HFHS diet displayed altered glucose tolerance during gestation  
100 (**Fig 1C**).

101 The offspring of HFHS-fed dams had heavier body weights at weaning and this elevated  
102 body weight persisted into adulthood (**Fig 1D**). We also evaluated body composition and found  
103 that adult animals born to obese dams displayed elevated fat and lean mass compared to  
104 control mice (**Fig 1E**). Moreover, neonatal exposure to HFHS caused adipocyte hypertrophy as  
105 revealed by a 1.5-fold increase in adipocyte size in epididymal white adipose tissue (**Fig 1F**).  
106 There was also an increase in food intake, and decreases in oxygen consumption ( $VO_2$ ) and  
107 energy expenditure in adult animals born to obese dams (**Fig 1G-I**). Respiratory exchange ratio  
108 and locomotor activity were not significantly different compared to controls (**Fig 1J and K**).  
109 However, adult mice born to obese dams displayed impaired glucose and insulin tolerances  
110 compared to mice born to lean dams (**Fig 1L and M**).

111

### 112 **Maternal obesity induces ER stress during postnatal development and neonatal TUDCA** 113 **treatment has long-term beneficial metabolic effects**

114 To examine if maternal obesity was associated with activation of ER stress response in the  
115 offspring, we measured the expression levels of the following ER stress markers in

116 metabolically-relevant tissues: activating transcription factor 4 (*Atf4*), 6 (*Atf6*), X-box binding  
117 protein (*Xbp1*), glucose regulated protein GRP78 (referred to as *Bip*), and CCAAT-enhancer-  
118 binding protein homologous protein (*Chop*), in P10 and adult animals born to chow- or HFHS-  
119 fed dams. The mRNA levels of *Atf4*, *Atf6*, *Xbp1*, *Bip*, and *Chop* were significantly elevated in the  
120 ARH of P10 mice born to obese dams (**Fig 2A**). Moreover, expression of *Atf4*, *Atf6*, *Xbp1*, and  
121 *Chop* mRNAs were significantly higher in the ARH of adult mice born to HFHS-fed dams (**Fig**  
122 **2B**). In contrast, only *Atf4* mRNA was significantly increased in the paraventricular nucleus  
123 (PVH) of P10 mice (**Fig 2C and D**). *Atf4*, *Atf6*, and *Xbp1* mRNAs were elevated in the pancreas  
124 of P10 pups of HFHS-fed dams (**Fig 2E**), but these markers were not significant changed in  
125 neonatal liver and fat tissues (**Fig 2G and I**). In addition, *Atf4*, *Atf6*, *Xbp1*, and *Chop* mRNA  
126 levels were higher in the pancreas of adult mice born to obese dams (**Fig 2F**), but only *Xbp1*  
127 and *Xbp1* as well as *Chop* mRNAs were significantly elevated in the liver and fat tissues,  
128 respectively, of adult mice of HFHS-fed dams (**Fig 2 H and J**).

129 To investigate the importance of early life ER stress, we treated pups born to HFHS-fed  
130 dams with daily peripheral injections of tauroursodeoxycholic acid (TUDCA) from P4 to P16,  
131 which represents a critical period for growth and development, including of the hypothalamus  
132 [2]. TUDCA is a chemical chaperone of low molecular weight that is well-known to alleviate ER  
133 stress [14,16]. Neonatal treatment with TUDCA in animals born to obese dams reversed  
134 induction of most ER stress markers in the postnatal and adult ARH, pancreas, liver, and  
135 adipose tissue (**Fig 2A-J**), with the exception of *Xbp1* in P10 ARH and pancreas (**Fig 2A and E**)  
136 and in adult pancreas (**Fig 2F**), and *Chop* in adult adipose tissue (**Fig 2J**). Neonatal TUDCA  
137 treatment also reduced normal mRNA levels of *Xbp1* in P10 PVH and liver (**Fig 2C and G**), *Bip*  
138 in P10 liver (**Fig 2G**), and *Atf6* in adult liver (**Fig 2H**). Physiologically, neonatal TUDCA  
139 treatment in animals born to obese dams reversed alterations in body weights, body  
140 composition, adipocytes, food intake, energy expenditure, and glucose and insulin tolerances  
141 (**Fig 1D-G, I, and L-M**), with only  $VO_2$  not being improved (**Fig 1H**).

142 Together, these data indicate that maternal obesity causes elevated ER stress levels in  
143 metabolically-relevant tissues during postnatal and adult life and that this induction of ER stress  
144 is reversible upon neonatal TUDCA treatment, which also causes long-term beneficial effects on  
145 energy metabolism.

146

147 **Maternal obesity causes hyperleptinemia and reduces hypothalamic leptin sensitivity in**  
148 **the offspring that is reversible with neonatal TUDCA treatment**

149 Previous studies have reported that during perinatal life leptin exerts marked  
150 neurodevelopmental and metabolic effects [8,17,18,19,20]. We therefore measured circulating  
151 leptin levels in animals exposed to maternal obesity. Maternal HFHS feeding was associated  
152 with a marked increase in serum leptin levels in dams at gestational day 16 and in E16.5  
153 embryos (**Fig 3A**). Serum leptin levels were also elevated in P10 pups born to obese dams,  
154 which were normalized upon neonatal TUDCA treatment (**Fig 3A**). However, serum leptin levels  
155 were unchanged in adult mice born to HFHS-fed mothers (**Fig 3A**). Because leptin's  
156 neurotrophic effects require intact ARH LepRb->pSTAT3 signaling [21], we also evaluated the  
157 number of pSTAT3-immunoreactive neurons after peripheral leptin injection and found that  
158 leptin treatment resulted in significantly fewer pSTAT3-positive cells in the ARH of P14 pups  
159 from obese dams and that neonatal TUDCA treatment enhanced ARH leptin-induced pSTAT3  
160 (**Fig 3B**). To determine whether maternal obesity affected leptin sensitivity in other hypothalamic  
161 nuclei, we also examined leptin-induced pSTAT3-immunoreactivity in the DMH and found that  
162 the number of pSTAT3-positive cells was unaltered in the DMH of pups born to HFHS-fed dams  
163 (**Fig 3B**).

164

165

166

167

168 **Neonatal TUDCA exposure restores disrupted POMC axonal projections in the offspring**  
169 **of HFHS-fed dams**

170 During postnatal development, neuronal projections from the ARH reach their target nuclei,  
171 including the PVH, under the influence of leptin and leptin receptor signaling [8,21]. Because our  
172 results indicate that maternal obesity alters offspring's leptin levels and ARH leptin signaling, we  
173 next investigated whether maternal obesity disrupts the development of ARH circuits by  
174 examining POMC and AgRP neuronal projections, two arcuate neuropeptidergic systems  
175 playing a critical role in energy balance. The density of POMC-immunoreactive fibers in the PVH  
176 of P14 mice born to obese dams was 2-fold lower than that observed in control mice (**Fig 4A**).  
177 In contrast, the density of AgRP-labeled projections innervating the PVH appeared normal in  
178 P14 pups born to HFHS-fed dams (**Fig 4A**). Also, the number POMC and NPY positive cells in  
179 the ARH of offspring of obese mice was comparable to that of control mice (**S1 Fig**). During  
180 adult life, both the densities of POMC- and AgRP-labeled fibers were reduced (**Fig 4B**). Similar  
181 decreases in POMC and AgRP fiber densities were also observed in the adult DMH, which is  
182 another terminal field of ARH projections (**S2 Fig**).

183 Because TUDCA treatment restores normal leptin signaling in the developing ARH, we  
184 also examined whether neonatal TUDCA treatment improved ARH projections. Neonatal  
185 injections of TUDCA in pups born to obese dams restored a normal density of POMC-labeled  
186 fibers in P14 pups born to obese dams (**Fig 4A**). However, enhancing ER capacity neonatally  
187 did not influence POMC or AgRP projections in adult animals (**Fig 4B and S2 Fig**)

188

189 **Maternal obesity increases circulating fatty acids concentration and treatment with**  
190 **saturated fatty acids induces ER stress and blunts ARH axonal outgrowth**

191 Our results show that overconsumption of a western-style diet rich in fatty acids during  
192 pregnancy and lactation is associated with abnormal hypothalamic development. We also  
193 measured circulating fatty acid concentration during pregnancy and found that dams fed a



194 HFHS diet have a 4-fold increase in serum fatty acid levels compared to control dams (**Fig 5A**).  
195 Offspring born to obese dams also displayed higher levels of circulating fatty acids at P10 that  
196 persisted into adulthood and neonatal TUDCA treatment restored normal levels of fatty acids  
197 (**Fig 5A**). To determine which type of fatty acids could cause neurodevelopmental abnormalities  
198 in our model, we reviewed the dietary fat content of the HFHS diet used in this study and found  
199 high concentrations (93.3%) of saturated fatty acids, including palmitic, lauric, and myristic acids  
200 and low concentrations (2.4%) of monounsaturated fats such as oleic acid (**Table 1**).

201 Direct exposure of N43/5 cells to individual saturated fatty acids such as palmitic, lauric,  
202 or myristic acids or a combination of these fatty acids increased ER stress markers gene  
203 expression (**S3 Fig**). In particular, the mRNA expression of *Atf4*, *Atf6*, *Xbp1*, *Bip*, and *Chop* was  
204 4- to 7-fold increased in cells treated with a combination of palmitic, lauric, and myristic acids  
205 compared to vehicle-treated cells (**Fig 5B**). In contrast, expression of ER stress markers was  
206 not affected when cells were treated with the monounsaturated fat oleic acid (**Fig 5B**).

207 We next assessed fatty acids intracellular transport in hypothalamic cells using BODIPY,  
208 a fluorescent long-chain fatty acids analog. Exposure of hypothalamic N43/5 cells to a  
209 combination of palmitic, lauric, and myristic acids resulted in greater BODIPY labeling in N43/5  
210 cell bodies compared to vehicle-treated cells (**Fig 5C**). In order to determine if these saturated  
211 fatty acids also impacted ARH axon growth and whether it involves ER stress, we also  
212 performed a series of *in vitro* experiments in which ARH explants were microdissected, placed  
213 in a collagen matrix, and then exposed to combination of saturated fatty acids (*i.e.*, palmitic,  
214 lauric, and myristic acids), or saturated fatty acids with TUDCA, or vehicle alone. After 48 hours,  
215 the density of TUJ1-labeled neurite, neuron-specific class III beta-tubulin, from ARH explants  
216 treated with saturated fatty acids was approximately 10-fold lower than that of vehicle-treated  
217 explants (**Fig 5D**). Moreover, pre-incubation of ARH explants with TUDCA improved disrupted  
218 axon outgrowth after saturated fatty acids treatment (**Fig 5D**).

219            Together, these data indicate that maternal obesity caused elevated circulating fatty acid  
220 levels in the dams and offspring and that direct exposure to saturated fatty acids induced ER  
221 stress gene expression in hypothalamic cells. They also show that saturated fatty acids can be  
222 transported in hypothalamic cells blunting axon growth, and that this phenomenon appears to  
223 involve ER stress pathways.

## 224 **Discussion**

225 Although the link between perinatal overnutrition and lifelong metabolic regulation has been  
226 clearly shown, little is known about the mechanisms underlying this programming effect. In this  
227 study, we show that maternal obesity causes lifelong metabolic alterations associated with  
228 abnormal development of hypothalamic feeding circuits in the offspring. We also report that  
229 maternal obesity induces ER stress in key tissues involved in energy metabolism during critical  
230 periods of growth and development, particularly in the arcuate nucleus and pancreas. Moreover,  
231 we found that relieving ER stress neonatally ameliorates metabolic and hypothalamic structural  
232 abnormalities in animals born to obese dams and that these effects are likely mediated through  
233 increased leptin sensitivity. Furthermore, we report that the malprogramming action of maternal  
234 obesity on hypothalamic development involves a direct effect of saturated fatty acids on arcuate  
235 axon growth.

236

237 Our findings are generally consistent with previous works showing that maternal obesity causes  
238 lifelong weight gain and glucose intolerance associated with disruption in AgRP/NPY and  
239 POMC axonal projections during adult life [10,11]. However, our study reveals that maternal  
240 obesity does not affect, during early postnatal life, AgRP circuits whereas it affects POMC  
241 axonal projections, suggesting that distinct mechanisms underlie the effects of maternal HFHS  
242 feeding on POMC *versus* AgRP/NPY neurons. Vogt and colleagues have specifically attempted  
243 to compare the consequences of maternal obesity during gestation and lactation and have  
244 shown that maternal consumption of HFD during lactation (but not during pregnancy) is  
245 sufficient to cause obesity and diabetes and to alter the development of POMC projections in  
246 the offspring [10]. Consistent with the importance of the postnatal period in the nutritional  
247 programming of metabolism and hypothalamic circuits, exposure to chronic postnatal  
248 overnutrition by rearing neonates in small litters also predisposes to obesity and disrupts  
249 hypothalamic development [22,23,24].

250

251 A variety of developmental pathways control the development of arcuate feeding circuits.  
252 Among this array of signals, attention has been given to leptin. The density of ARH axonal  
253 projections is reduced in leptin-deficient mouse neonates and adults, which can be rescued with  
254 leptin treatment during early postnatal life [8,25,26]. Moreover, leptin appears to exert its  
255 neurodevelopmental actions on arcuate circuits through LepRb→pSTAT3 signaling [21]. The  
256 data presented here indicate that maternal obesity causes chronic hyperleptinemia in the  
257 offspring associated with reduced arcuate leptin-induced pSTAT3 during a critical period of  
258 hypothalamic development. A similar increase in circulating leptin levels and a reduction in  
259 arcuate leptin sensitivity has been reported in rat neonates exposed to chronic postnatal  
260 overnutrition [22]. However, the mechanisms underlying this early leptin resistance remained  
261 elusive. Here, we show that relieving ER stress enhances arcuate leptin resistance and  
262 improves hypothalamic development and long-term metabolic outcomes. These findings are  
263 consistent with previous data showing that ER stress inducers, such as tunicamycin, blunts  
264 neurite elongation and induce a collapse of neuronal growth cones from PC-12 cells or  
265 dissociated rat sensory neurons [27]. The site of action of TUDCA remains to be determined but  
266 it likely involves a direct effect on ARH neurons. The highest level of ER stress induction is  
267 observed in the ARH and neonatal TUDCA treatment normalizes arcuate ER stress gene  
268 expression. Moreover, previous studies have reported that the pharmacological induction and  
269 genetic loss of the ER stress function in the brain block hypothalamic leptin-induced STAT3  
270 activation [14].

271

272 Future studies are needed to determine the contribution of specific ER stress pathways to the  
273 nutritional programming of hypothalamic development and leptin resistance. However, previous  
274 studies have shown that overexpression of *Xbp1* or *Atf6* in mouse embryonic fibroblast cells  
275 increases their resistance to the inhibitory effects of tunicamycin and prevents ER stress-

276 mediated inhibition of leptin signaling [14]. Moreover, when fed a high fat diet, mice lacking  
277 *Xbp1* in neurons display an obesogenic phenotype, associated with hyperphagia and reduced  
278 oxygen consumption [14]. In addition, leptin-induced STAT3 phosphorylation is significantly  
279 attenuated in the hypothalamus of these mice [14]. Furthermore, constitutive expression of a  
280 dominant *Xbp1* form specifically in POMC neurons leads to a lean phenotype, characterized by  
281 increased energy expenditure and leptin sensitivity, further supporting a fundamental role for the  
282 XBP1 pathway in POMC neurons in the deleterious metabolic effects of hypothalamic ER  
283 stress [15].

284

285 Our results show that lipid overload, especially saturated fatty acids, triggers ER stress in  
286 hypothalamic cells and that it contributes to disruption in arcuate axon growth. Previous studies  
287 have demonstrated that hypothalamic neurons can sense circulating fatty acids, and that  
288 endogenous lipid metabolism in the hypothalamus is a key mechanism regulating whole-body  
289 energy balance [28]. Adult rodents fed a HFD exhibit elevated concentrations of fatty acids in  
290 the hypothalamus, which causes an accumulation of palmitoyl-CoA and other harmful species  
291 [29,30]. Moreover, studies in hypothalamic cell lines have demonstrated that palmitate triggers  
292 ER stress and apoptosis [31,32,33]. In addition, intracerebroventricular injection of saturated  
293 fatty acids *in vivo* induces ER stress in the hypothalamus of rats [34]. Notably, palmitate  
294 decreases protein abundance and function of the  $\alpha$ -MSH receptor MC4-R and chemical  
295 chaperone reverses this biochemical abnormality [35], suggesting that saturated fatty acids may  
296 not only cause disruption in the development of POMC axonal projections, but also attenuate  
297 the post-synaptic action of POMC-derived peptides through a ER stress-dependent mechanism.

298 **Methods**

299 **Animals**

300 All animal procedures were conducted in compliance with and approved by the IACUC of the  
301 Saban Research Institute of the Children's Hospital of Los Angeles. The animals were housed  
302 under specific pathogen-free conditions, maintained in a temperature-controlled room with a 12  
303 h light/dark cycle, and provided *ad libitum* access to water and standard laboratory chow  
304 (Special Diet Services). At 7 weeks of age, female C57BL/6J wild-type (WT) mice were placed  
305 on either a regular chow diet [4.5 kcal% fat, provided by PicoLab Rodent Diet 5053] or a high-  
306 fat, high-sugar (HFHS) diet [58 kcal% fat with sucrose, provided by Research Diet D12331] for 6  
307 weeks before mating. The mice were kept on their respective diets throughout pregnancy and  
308 lactation. Male breeders were fed a normal chow diet. Offspring were fed a normal chow diet  
309 after weaning. Litter sizes were standardized to six pups 48 hours post-delivery, and attempts  
310 were made to maintain an equal sex ratio. Only male mice were studied.

311

312 **Neonatal TUDCA treatment**

313 The mice were injected intraperitoneally daily with TUDCA (Millipore, 150 mg/kg/day) from P4 to  
314 P16. Controls received injections with an equivalent volume of vehicle (0.9% NaCl).

315

316 **Tissue collection**

317 The ARH and PVH of P10 and 10-week-old mice were dissected under a stereomicroscope.  
318 Liver, pancreas and epididymal white adipose tissues were collected from P10 and 10-week-old  
319 mice.

320

321 **Cell culture and fatty acid treatment**

322 The embryonic mouse hypothalamic cell line N43/5 was cultured in Dulbecco's modified Eagle's  
323 medium (Sigma, D5796) supplemented with 10% fetal bovine serum, 100 U/ml penicillin and

324 100 µg/ml streptomycin at 37°C in 5% CO<sub>2</sub> and a humidified atmosphere. N43/5 cells were  
325 plated out at density of 6x10<sup>5</sup> cells per well in a 6-wells plate. The following day, medium was  
326 changed to culture medium containing either vehicle (BSA with 0.1% ethanol; Sigma), or  
327 palmitic (PA; 250 µM; Sigma), lauric (LA; 1mM; Sigma), myristic (MA; 200 µM; Sigma), or oleic  
328 acids (OA; 250 µM; Sigma), or combination of these fatty acids for 24h.

329

### 330 **RNA extraction and RT-qPCR analyses**

331 Total RNA was isolated using the Arcturus PicoPure RNA Isolation Kit (for hypothalamic  
332 samples) (Life Technologies), the RNeasy Lipid Tissue Kit (for peripheral samples) (Qiagen), or  
333 PureLink RNA mini kit (for N43/5 cell samples). cDNA was generated with the High-Capacity  
334 cDNA Reverse Transcription Kit (Life Technologies). Quantitative real-time PCR was performed  
335 using TaqMan Fast Universal PCR Master Mix and the commercially available TaqMan gene  
336 expression primers: *Atf4* (Mm00515324\_m1), *Atf6* (Mm01295317\_m1), *Xbp1*  
337 (Mm00457357\_m1) *Bip* (Mm00517691\_m1), *Chop* (Mm00492097\_m1), and *Gapdh*  
338 (Mm99999915\_g1). mRNA expression was calculated using the 2<sup>-ΔΔCt</sup> method after  
339 normalization to the expression of the *Gapdh* housekeeping gene. All assays were performed  
340 using an Applied Biosystems 7900 HT real-time PCR system.

341

### 342 **Physiological measures**

343 The maternal body weight was recorded weekly until the end of pregnancy. Offspring (n = 5 per  
344 group) was weighed weekly 1 to 10 weeks of age using an analytical balance. Body composition  
345 analysis (fat/lean mass) was performed in pregnant females at gestational day 16 and in the  
346 offspring at 10 weeks of age using NMR (Echo MRI). Food intake, O<sub>2</sub> and CO<sub>2</sub> production,  
347 energy expenditure, respiratory exchange ratio (*i.e.*, VCO<sub>2</sub>/O<sub>2</sub>), and locomotor activity (XY) were  
348 monitored at 10 weeks of age using a combined indirect calorimetry system (TSE Systems).  
349 The mice were acclimated in monitoring chambers for 2 days, and the data were collected for 3

350 days. These physiological measures were performed at the Rodent Metabolic Core of Children's  
351 Hospital of Los Angeles.

352 Glucose and insulin tolerance tests (GTT and ITT) were conducted in 7-8-week-old mice  
353 through i.p. injection of glucose (1.5 mg/g body weight) or insulin (2U/kg body weight) after  
354 overnight fasting. Blood glucose levels were measured at 0, 15, 30, 45, 60, 90, 120, and 150  
355 min post-injection, as previously described [36].

356 Serum leptin levels were assayed in chow-fed or HFHS-fed mothers at gestational day  
357 16, and in the offspring of chow- or HFHS-fed dams at E16.5, P10 and 10 weeks of age using a  
358 commercially available leptin ELISA kit (Millipore). Serum free fatty acid levels were assayed in  
359 chow-fed or HFHS-fed mothers at gestational day 16 and in the offspring of chow- or HFHS-fed  
360 dams at P10 and 10 weeks of age using a commercially available FFA kit (Abcam).

361

### 362 **POMC, AgRP, and NPY immunohistochemistry**

363 Ten- to 12-week-old mice were perfused transcardially with 4% paraformaldehyde. The brains  
364 were then frozen, sectioned at 30- $\mu$ m thick, and processed for immunofluorescence using  
365 standard procedures [8,37]. The primary antibodies used for IHC were as follows: rabbit anti-  
366 POMC (1:20,000, Phoenix Pharmaceuticals), rabbit anti-AgRP (1:1,000, Phoenix  
367 Pharmaceuticals), and sheep anti-NPY (1:3,000, Abcam). The primary antibodies were  
368 visualized with Alexa Fluor 647 donkey anti-sheep IgG, Alexa Fluor 488 donkey anti-rabbit IgG,  
369 or Alexa Fluor 488 donkey anti-mouse IgG, or Alexa Fluor 568 donkey anti-rabbit IgG (1:200,  
370 Millipore). The sections were counterstained using bis-benzamide (1:10,000, Invitrogen) to  
371 visualize cell nuclei.

372

373

374

375



376 **pSTAT3 immunohistochemistry**

377

378 Leptin (3 mg/kg; Peprotech) was injected intraperitoneally in P14 pups. Animals were perfused  
379 45 min later with a solution of 2% paraformaldehyde. Frozen coronal sections were cut at 30  $\mu$ m  
380 and pretreated for 20 min in 0.5% NaOH and 0.5% H<sub>2</sub>O<sub>2</sub> in KPBS, followed by immersion in  
381 0.3% glycine for 10 min. Sections were then placed in 0.03% SDS for 10 min and placed in 4%  
382 normal serum + 0.4% Triton X-100 + 1% BSA (fraction V) for 20 min before incubation for 48h  
383 with a rabbit anti-pSTAT3 antibody (1:1,000, Cell Signaling). The primary antibody was localized  
384 with Alexa Fluor 568 Goat anti-Rabbit IgGs (Invitrogen; 1:200). Sections were counterstained  
385 using bis-benzamide (Invitrogen; 1:10,000) to visualize cell nuclei, and coverslipped with  
386 buffered glycerol (pH 8.5).

387

388 **Histomorphological assessment of white adipose tissue**

389 Epididymal white adipose tissue from 10-weekold mice was collected, fixed in a 4%  
390 paraformaldehyde solution, sectioned at 5  $\mu$ m, and then stained with a Perilipin A antibody  
391 (1:1,000, Sigma) using standard procedures.

392

393 **BODIPY staining**

394 N43/5 cells were treated with vehicle or a combination of palmitate (250  $\mu$ M; Sigma) with lauric  
395 (1mM; Sigma) and myristic acids (200  $\mu$ M; Sigma) for 24 hr and 2  $\mu$ M of Bodipy 493/503 (4,4-  
396 difluoro-1,3,5,7-tetramethyl-4-bora-3a,4a-diaza-s-indacene; Invitrogen) and Alexa Fluor 568  
397 Phalloidin (0.1  $\mu$ M; Invitrogen) were added to culture media for 15 min at room temperature.  
398 N43/5 were then fixed in a solution of 4% paraformaldehyde for 5 min and washed with KPBS.  
399 Slides were counterstained using bis-benzamide (Invitrogen; 1:10,000) to visualize cell nuclei.

400

401

## 402 **Isolated ARH explant culture**

403 Brains were collected from P4 mice and sectioned at a 200- $\mu\text{m}$  thickness with a vibroslicer as  
404 previously described [8,37]. The ARH was then carefully dissected out of each section under a  
405 stereomicroscope. Explants were cultured onto a rat tail collagen matrix (BD Bioscience) and  
406 each explant was pre-treated for 6 h with fresh modified Basal Medium Eagle (Invitrogen)  
407 containing TUDCA (750 $\mu\text{g}/\text{ml}$ ) or vehicle followed by a combination of palmitate (250  $\mu\text{M}$ ) with  
408 lauric (1mM) and myristic acids (200  $\mu\text{M}$ ) or vehicle alone (BSA with 0.1% ethanol). After 48 h,  
409 the explants were fixed in paraformaldehyde and neurites extending from the explants were  
410 stained with TUJ1 ( $\beta$  III tubulin) (rabbit, 1:5,000, Covance) as described previously [37].

411

## 412 **Image analysis**

413 The images were acquired using a Zeiss LSM 710 confocal system equipped with a 20X  
414 objective through the ARH (for cell numbers), through the PVH and the DMH (for fibers density),  
415 through adipose tissue (for adipocyte size), and through N43/5 cell cultures (for BODIPY  
416 staining). The average number of cells and density of fibers were analyzed in 2-4 sections per  
417 culture. For the explant experiments, sections were acquired using a Zeiss LSM 710 confocal  
418 system equipped with a 10X objective. Slides were numerically coded to obscure the treatment  
419 group. The image analysis was performed using ImageJ analysis software (NIH) as previously  
420 described [21,36,37].

421 For the quantitative analysis of cell number, POMC<sup>+</sup>, NPY<sup>+</sup>, and pSTAT3<sup>+</sup> cells were  
422 manually counted. Only cells with corresponding bis-benzamide-stained nuclei were included in  
423 our counts.

424 Determination of mean adipocyte size ( $\mu\text{m}^2$ ) was measured semi-automatically using the  
425 FIJI distribution [30] of Image J software (NIH, ImageJ1.47i). The average adipocyte size  
426 measured from 3 fields and six sections in each mouse was used for statistical comparisons  
427 used for statistical comparisons.

428

429 For the quantitative analysis of fiber density (for POMC, AgRP, and TUJ1 fibers) and  
430 BODIPY fluorescence, each image plane was binarized to isolate labeled materials from the  
431 background and to compensate for differences in fluorescence intensity. The integrated  
432 intensity, which reflects the total number of pixels in the binarized image, was then calculated  
433 for each image as previously described [8,37]. This procedure was conducted for each image  
434 plane in the stack, and the values for all of the image planes in a stack were summed.

435

#### 436 **Statistical analysis**

437 All values are represented as the mean  $\pm$  SEM. Statistical analyses were conducted using  
438 GraphPad Prism (version 5.0a). Data sets with only two independent groups were analyzed for  
439 statistical significance using unpaired two-tailed Student's t test. Data sets with more than two  
440 groups were analyzed using one-way analysis of variance (ANOVA) followed by the Tukey's  
441 Multiple Comparison test. For statistical analyses of body weight, GTT ITT, and RER, we  
442 performed two-way ANOVAs followed by Tukey's Multiple Comparison test. Statistically  
443 significant outliers were calculated using Grubb's test for outliers.  $P \leq 0.05$  was considered  
444 statistically significant.

445

#### 446 **Supplementary material**

447 Supplementary material includes 3 figures and can be found with this article online.

448 **Acknowledgments**

449 We thank Brad Wanken and the CHLA Rodent Metabolic Core for metabolic studies. We also  
450 thank the CHLA Cellular Imaging Core for confocal imaging studies. We are also grateful to  
451 Gricelda Vasquez for her assistance with animal husbandry. This study was supported by the  
452 National Institutes of Health (Grants DK84142, DK102780, and DK118401 to SGB).

453

454 **Author Contributions**

455 S.P. conceived, designed, and performed most of the experiments and analyzed the data. A.J.  
456 performed and analyzed some of the immunohistochemical experiments. S.G.B. conceived,  
457 designed, and supervised the project. S.P. and S.G.B. wrote the manuscript.

458

459 **Competing Interest statements**

460 The authors declare no competing interests.

461

## 462 References

- 463 1. McMillen IC, Adam CL, Muhlhausler BS (2005) Early origins of obesity: programming the  
464 appetite regulatory system. *J Physiol (Lond)* 565: 9-17.
- 465 2. Bouret S, Levin BE, Ozanne SE (2015) Gene-Environment Interactions Controlling Energy  
466 and Glucose Homeostasis and the Developmental Origins of Obesity. 47-82 p.
- 467 3. Sullivan EL, Grove KL (2010) Metabolic imprinting in obesity. *Forum Nutr* 63: 186-194.
- 468 4. Taylor PD, Poston L (2007) Developmental programming of obesity in mammals. *Exp Physiol*  
469 92: 287-298.
- 470 5. Martin-Gronert MS, Ozanne SE (2005) Programming of appetite and type 2 diabetes. *Early*  
471 *Human Development* 81: 981-988.
- 472 6. Horvath TL, Bruning JC (2006) Developmental programming of the hypothalamus: a matter of  
473 fat. *Nat Med* 12: 52-53.
- 474 7. Chen H, Simar D, Morris MJ (2009) Hypothalamic Neuroendocrine Circuitry is Programmed  
475 by Maternal Obesity: Interaction with Postnatal Nutritional Environment. *PLoS ONE* 4:  
476 e6259.
- 477 8. Bouret SG, Draper SJ, Simerly RB (2004) Trophic Action of Leptin on Hypothalamic Neurons  
478 That Regulate Feeding. *Science* 304: 108-110.
- 479 9. Bouret SG, Gorski JN, Patterson CM, Chen S, Levin BE, et al. (2008) Hypothalamic Neural  
480 Projections Are Permanently Disrupted in Diet-Induced Obese Rats. *Cell Metabolism* 7:  
481 179-185.
- 482 10. Vogt MC, Paeger L, Hess S, Steculorum SM, Awazawa M, et al. (2014) Neonatal Insulin  
483 Action Impairs Hypothalamic Neurocircuit Formation in Response to Maternal High-Fat  
484 Feeding. *Cell* 156: 495-509.
- 485 11. Kirk SL, Samuelsson A-M, Argenton M, Dhonye H, Kalamatianos T, et al. (2009) Maternal  
486 Obesity Induced by Diet in Rats Permanently Influences Central Processes Regulating  
487 Food Intake in Offspring. *PLoS ONE* 4: e5870.
- 488 12. Ozcan U, Cao Q, Yilmaz E, Lee A-H, Iwakoshi NN, et al. (2004) Endoplasmic Reticulum  
489 Stress Links Obesity, Insulin Action, and Type 2 Diabetes. *Science* 306: 457-461.
- 490 13. Özcan U, Yilmaz E, Özcan L, Furuhashi M, Vaillancourt E, et al. (2006) Chemical  
491 Chaperones Reduce ER Stress and Restore Glucose Homeostasis in a Mouse Model of  
492 Type 2 Diabetes. *Science* 313: 1137-1140.
- 493 14. Ozcan L, Ergin AS, Lu A, Chung J, Sarkar S, et al. (2009) Endoplasmic reticulum stress  
494 plays a central role in development of leptin resistance. *Cell Metab* 9: 35-51.
- 495 15. Williams KW, Liu T, Kong X, Fukuda M, Deng Y, et al. (2014) Xbp1s in Pomc neurons  
496 connects ER stress with energy balance and glucose homeostasis. *Cell Metab* 20: 471-  
497 482.
- 498 16. Perlmutter DH (2002) Chemical chaperones: a pharmacological strategy for disorders of  
499 protein folding and trafficking. *Pediatr Res* 52: 832-836.
- 500 17. Attig L, Solomon G, Ferezou J, Abdennebi-Najar L, Taouis M, et al. (2008) Early postnatal  
501 leptin blockage leads to a long-term leptin resistance and susceptibility to diet-induced  
502 obesity in rats. *Int J Obes* 32: 1153-1160.
- 503 18. Yura S, Itoh H, Sagawa N, Yamamoto H, Masuzaki H, et al. (2005) Role of premature leptin  
504 surge in obesity resulting from intrauterine undernutrition. *Cell Metabolism* 1: 371-378.
- 505 19. Vickers MH, Gluckman PD, Coveny AH, Hofman PL, Cutfield WS, et al. (2005) Neonatal  
506 Leptin Treatment Reverses Developmental Programming. *Endocrinology* 146: 4211-  
507 4216.
- 508 20. Vickers MH, Gluckman PD, Coveny AH, Hofman PL, Cutfield WS, et al. (2008) The Effect of  
509 Neonatal Leptin Treatment on Postnatal Weight Gain in Male Rats Is Dependent on  
510 Maternal Nutritional Status during Pregnancy. *Endocrinology* 149: 1906-1913.

- 511 21. Bouret SG, Bates SH, Chen S, Myers MG, Simerly RB (2012) Distinct Roles for Specific  
512 Leptin Receptor Signals in the Development of Hypothalamic Feeding Circuits. *The*  
513 *Journal of Neuroscience* 32: 1244-1252.
- 514 22. Glavas MM, Kirigiti MA, Xiao XQ, Enriori PJ, Fisher SK, et al. (2010) Early Overnutrition  
515 Results in Early-Onset Arcuate Leptin Resistance and Increased Sensitivity to High-Fat  
516 Diet. *Endocrinology* 151: 1598-1610.
- 517 23. Collden G, Balland E, Parkash J, Caron E, Langlet F, et al. (2015) Neonatal overnutrition  
518 causes early alterations in the central response to peripheral ghrelin. *Molecular*  
519 *Metabolism* 4: 15-24.
- 520 24. Caron E, Ciofi P, Prevot V, Bouret SG (2012) Alteration in Neonatal Nutrition Causes  
521 Perturbations in Hypothalamic Neural Circuits Controlling Reproductive Function. *J*  
522 *Neurosci* in press.
- 523 25. Bouyer K, Simerly RB (2013) Neonatal Leptin Exposure Specifies Innervation of  
524 Presympathetic Hypothalamic Neurons and Improves the Metabolic Status of Leptin-  
525 Deficient Mice. *The Journal of Neuroscience* 33: 840-851.
- 526 26. Kamitakahara A, Bouyer K, Wang CH, Simerly R (2017) A critical period for the trophic  
527 actions of leptin on AgRP neurons in the arcuate nucleus of the hypothalamus. *J Comp*  
528 *Neurol*.
- 529 27. Patterson S, Skene J (1994) Novel inhibitory action of tunicamycin homologues suggests a  
530 role for dynamic protein fatty acylation in growth cone-mediated neurite extension. *The*  
531 *Journal of Cell Biology* 124: 521-536.
- 532 28. Martinez de Morentin PB, Varela L, Ferno J, Nogueiras R, Dieguez C, et al. (2010)  
533 Hypothalamic lipotoxicity and the metabolic syndrome. *Biochim Biophys Acta* 1801: 350-  
534 361.
- 535 29. Benoit SC, Kemp CJ, Elias CF, Abplanalp W, Herman JP, et al. (2009) Palmitic acid  
536 mediates hypothalamic insulin resistance by altering PKC- $\theta$  subcellular localization  
537 in rodents. *J Clin Invest* 119: 2577-2589.
- 538 30. Posey KA, Clegg DJ, Printz RL, Byun J, Morton GJ, et al. (2009) Hypothalamic  
539 proinflammatory lipid accumulation, inflammation, and insulin resistance in rats fed a  
540 high-fat diet. *Am J Physiol Endocrinol Metab* 296: E1003-1012.
- 541 31. Mayer CM, Belsham DD (2010) Palmitate attenuates insulin signaling and induces  
542 endoplasmic reticulum stress and apoptosis in hypothalamic neurons: rescue of  
543 resistance and apoptosis through adenosine 5' monophosphate-activated protein kinase  
544 activation. *Endocrinology* 151: 576-585.
- 545 32. Choi SJ, Kim F, Schwartz MW, Wisse BE (2010) Cultured hypothalamic neurons are  
546 resistant to inflammation and insulin resistance induced by saturated fatty acids. *Am J*  
547 *Physiol Endocrinol Metab* 298: E1122-1130.
- 548 33. McFadden JW, Aja S, Li Q, Bandaru VV, Kim EK, et al. (2014) Increasing fatty acid  
549 oxidation remodels the hypothalamic neurometabolome to mitigate stress and  
550 inflammation. *PLoS One* 9: e115642.
- 551 34. Milanski M, Degasperi G, Coope A, Morari J, Denis R, et al. (2009) Saturated fatty acids  
552 produce an inflammatory response predominantly through the activation of TLR4  
553 signaling in hypothalamus: implications for the pathogenesis of obesity. *J Neurosci* 29:  
554 359-370.
- 555 35. Cragle FK, Baldini G (2014) Mild lipid stress induces profound loss of MC4R protein  
556 abundance and function. *Mol Endocrinol* 28: 357-367.
- 557 36. Coupe B, Ishii Y, Dietrich MO, Komatsu M, Horvath TL, et al. (2012) Loss of Autophagy in  
558 Pro-opiomelanocortin Neurons Perturbs Axon Growth and Causes Metabolic  
559 Dysregulation. *Cell Metabolism* 15: 247-255.

560 37. Steculorum SM CG, Coupe B, Croizier S, Andrews Z, Jarosch F, Klusmann S, Bouret SG.  
561 (2015) Ghrelin programs development of hypothalamic feeding circuits. . The Journal of  
562 Clinical Investigation 125: 846–858.

563

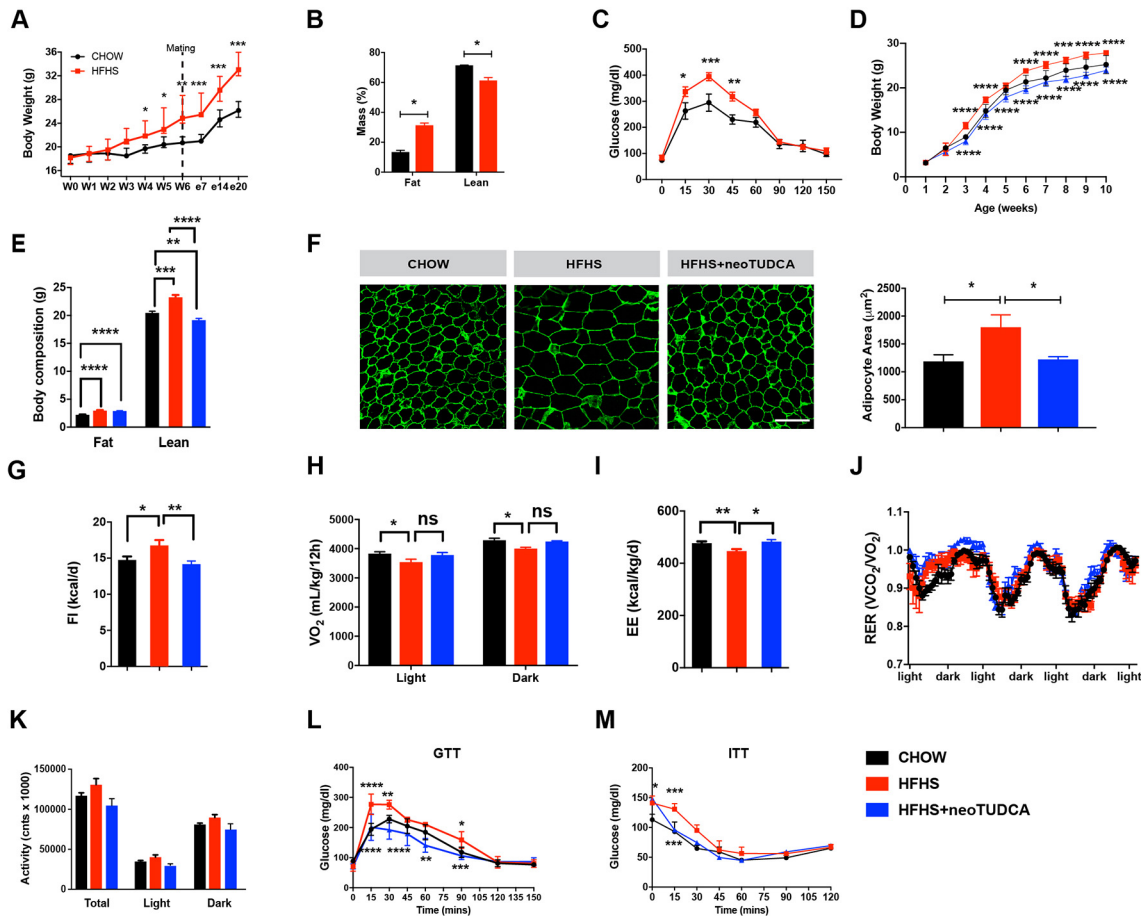
564 **Table 1.** Fatty acid composition of D12331 diet

<b>Fatty acid</b>	<b>gm/kg diet</b>
C6, Caproic	2.0
C8, Caprylic	25.7
C10, Capric	19.7
C12, Lauric	158.7
C14, Myristic	60.0
C16, Palmitic	31.6
C18, Stearic	36.3
C18:1, Oleic	8.7
C18:2, Linoleic	13.5
C18:3, Linolenic	2.0

565

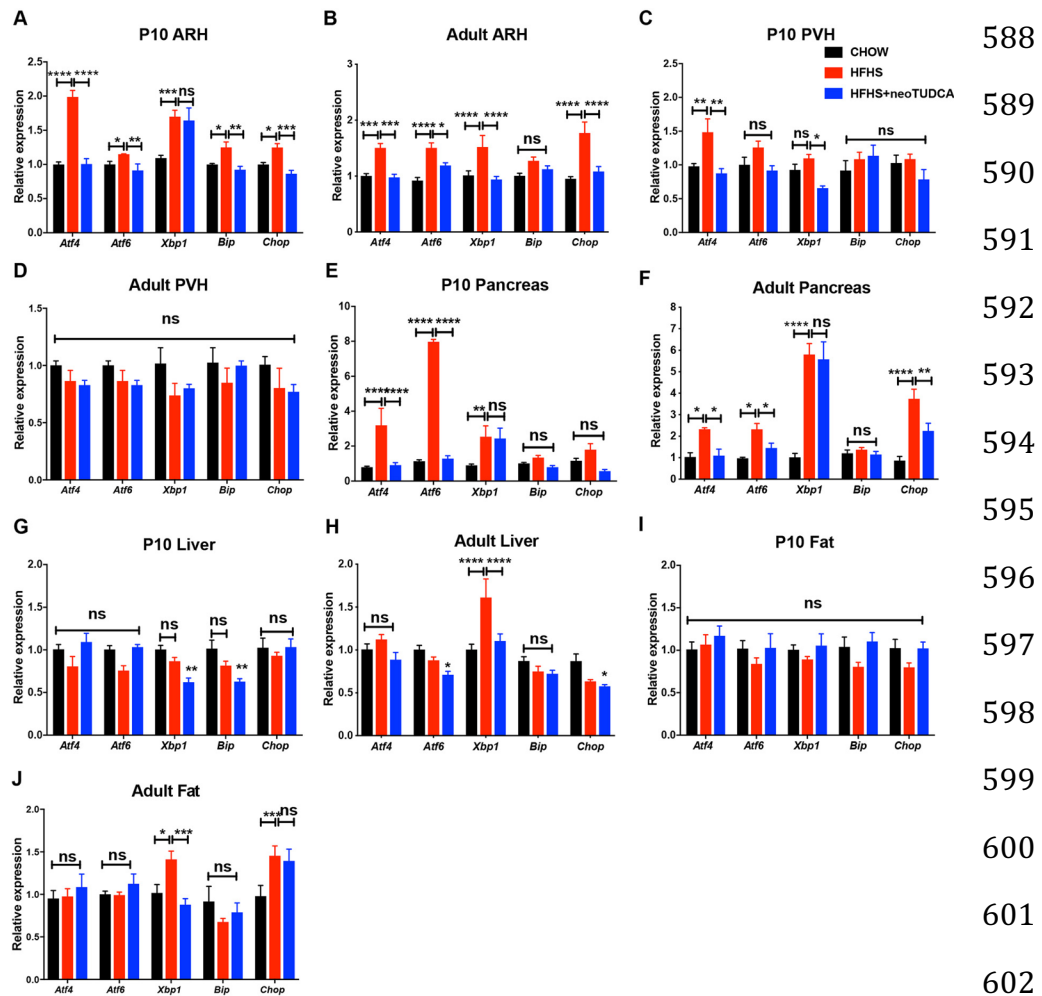


566 **Figures and Figure Legends**

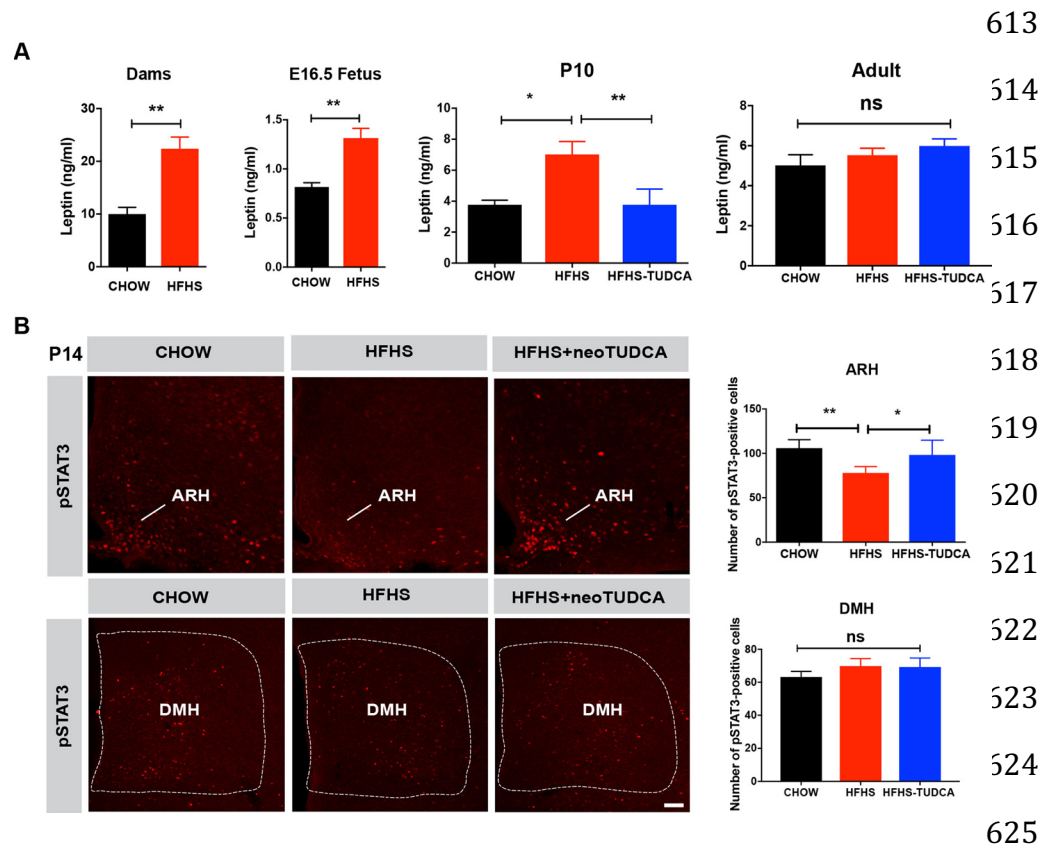


567 **Fig 1. Maternal obesity impairs energy balance and glucose homeostasis in the offspring**  
 568 **and neonatal TUDCA treatment improves this metabolic malprogramming.** (A) Body  
 569 weight curves of adult female mice fed a chow or a high-fat high-sucrose (HFHS) diet before  
 570 and during pregnancy (n = 5 per group). (B) Body composition (n = 3 per group) and (C)  
 571 glucose tolerance test (GTT) (n = 4-5 per group) of pregnant female mice fed a chow or HFHS  
 572 diet at gestational day 16. (D) Body weight curves of mice born to chow-fed dams, HFHS-fed  
 573 dams, or HFHS-fed dams and treated with tauroursodeoxycholic acid (TUDCA) neonatally  
 574 (neoTUDCA) (n = 5-10 per group). (E) Average body composition (n = 5-8 per group) and (F)  
 575 representative images and quantification of adipocyte size (immunostained for perilipin, *green*  
 576 fluorescence) of 10-week-old mice born to chow-fed dams, HFHS-fed dams, or HFHS-fed dams

577 and treated with TUDCA neonatally (n =4-5 per group). (G) Food intake, (H) oxygen  
578 consumption, (I) energy expenditure, (J) respiratory exchange ratio (RER), and (K) locomotor  
579 activity of 10-week-old mice born to chow-fed dams, HFHS-fed dams, or HFHS-fed dams and  
580 treated with TUDCA neonatally (n = 3-8 per group). (L) Glucose (GTT) and (M) insulin tolerance  
581 tests (ITT) of 7-8-week-old mice born to chow-fed dams, HFHS-fed dams, or HFHS-fed dams  
582 and treated with TUDCA neonatally (n = 4-8 per group). Data are presented as mean  $\pm$  SEM. \**P*  
583  $\leq$  0.05, \*\**P*  $\leq$  0.01, \*\*\**P*  $\leq$  0.001, and \*\*\*\**P*  $\leq$  0.0001 *versus* chow groups. Statistical significance  
584 between groups was determined by unpaired two-tailed Student's *t* test (E), one-way ANOVA  
585 (F, I, K), and two-way ANOVA (A-D, H, L, M) followed by Tukey's Multiple Comparison test.  
586 Scale bar, 100  $\mu$ m.  
587



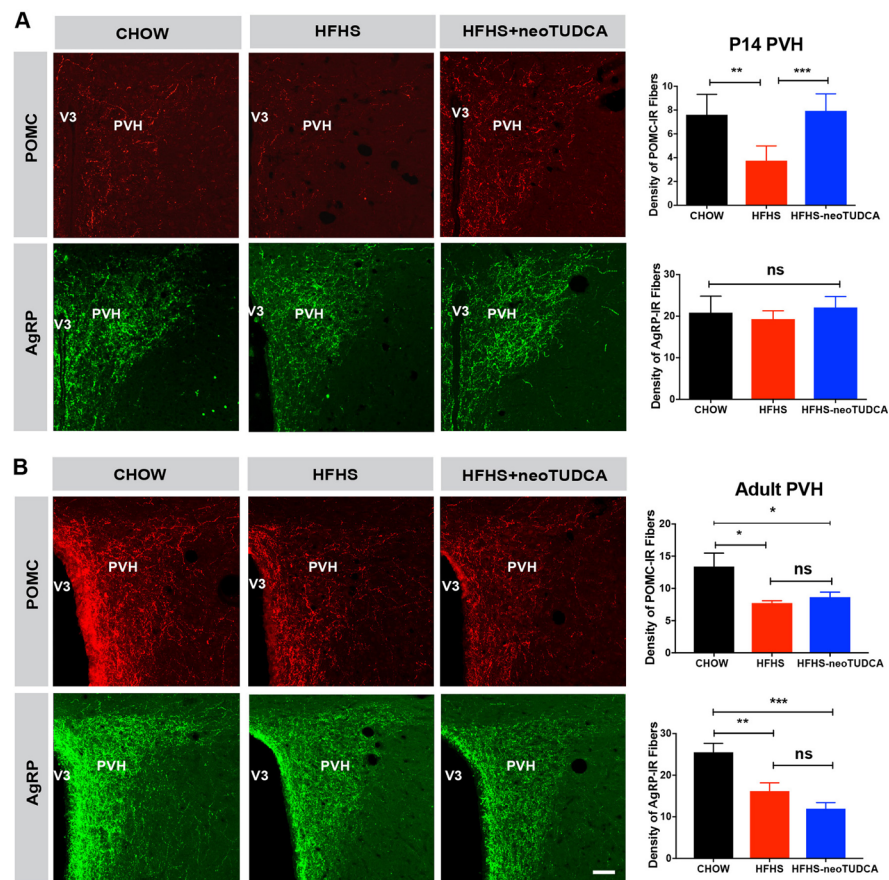
603 **Fig 2. Neonatal TUDCA treatment reverses the elevated expression of ER stress markers**  
 604 **in the offspring of obese dams. (A-J)** Relative expression of *Atf4*, *Atf6*, *Xbp1*, *Bip*, and *Chop*  
 605 mRNA in (A, B) the arcuate nucleus (ARH), (C, D) paraventricular nucleus (PVH), (E, F)  
 606 pancreas, (G, H) liver, and (I, J) fat depot of (A, C, E, G, and I) P10 and (B, D, F, H, and J) 10-  
 607 week-old adult mice born to chow-fed dams, high-fat high-sucrose (HFHS)-fed dams, or HFHS-  
 608 fed dams and treated with TUDCA neonatally (n = 4-6 per group). Data are presented as mean  
 609 ± SEM. \**P* ≤ 0.05, \*\**P* < 0.01, \*\*\**P* ≤ 0.001, and \*\*\*\**P* ≤ 0.0001 versus other groups. Statistical  
 610 significance between groups was determined by two-way ANOVA (A-J) followed by Tukey's  
 611 Multiple Comparison test.  
 612



626 **Fig 3. Maternal obesity causes neonatal hyperleptinemia and attenuated response to**  
 627 **leptin that can be reversed by neonatal TUDCA treatment.** (A) Serum leptin levels in dams  
 628 at gestational day 16 and E16.5 fetuses of dams fed a chow or HFHS diet and in P10 and 10-  
 629 week-old mice born to chow-fed dams, high-fat high-sucrose (HFHS)-fed dams, or HFHS-fed  
 630 dams and treated with TUDCA neonatally (n = 4-8 per group). (B) Confocal images and  
 631 quantification of the number of leptin-induced pSTAT3-immunoreactive cells in the arcuate  
 632 nucleus (ARH) and dorsomedial nucleus (DMH) of P14 pups born to chow-fed dams, HFHS-fed  
 633 dams, or HFHS-fed dams and treated with TUDCA neonatally (n = 5 per group). Data are  
 634 presented as mean  $\pm$  SEM. \* $P \leq 0.05$  and \*\* $P < 0.01$  versus chow groups. Statistical  
 635 significance was determined by unpaired two-tailed Student's t test (A), and one-way ANOVA  
 636 followed by Tukey's Multiple Comparison test (B). Scale bar, 100  $\mu$ m.

637

638



639 **Fig 4. TUDCA treatment reverses neonatal disruption of POMC axonal projections**  
 640 **induced by maternal obesity.** Confocal images and quantification of the density of pro-  
 641 opiomelanocortin (POMC)- and agouti-related peptide (AgRP)-immunoreactive fibers in the  
 642 paraventricular nucleus (PVH) of (A) P14 and (B) 10- to 12-week-old mice born to chow-fed  
 643 dams, HFHS-fed dams, or HFHS-fed dams and treated with TUDCA neonatally (n = 5-7 per  
 644 group). Data are presented as mean  $\pm$  SEM. \* $P \leq 0.05$ , \*\* $P < 0.01$ , \*\*\* $P \leq 0.001$ , and \*\*\*\* $P \leq$   
 645 0.0001 versus other groups. Statistical significance was determined by one-way ANOVA (A-B)  
 646 followed by Tukey's Multiple Comparison test. ARH, arcuate nucleus of the hypothalamus; PVH,  
 647 paraventricular nucleus of the hypothalamus. Scale bar, 50  $\mu$ m.

648

649

650

651

652

653

654

655

656

657

658

659

660

661

662

663

664 **Fig 5. Saturated fatty acid treatment causes ER stress-induced disruption of axon**

665 **growth.** (A) Serum fatty acid levels in dams, P10 and 10-week-old mice born to chow-fed dams,

666 HFHS-fed dams, or HFHS-fed dams and treated with TUDCA neonatally (n = 4-7 per group). (B)

667 Relative expression of *Atf4*, *Atf6*, *Xbp1*, *Bip*, and *Chop* mRNA in mouse hypothalamic N43/5

668 cells treated with vehicle (BSA with 0.1% ethanol), or a cocktail of palmitate (250  $\mu$ M) with lauric

669 (1mM) and myristic acids (200  $\mu$ M) (PA+LA+MA), or oleic acid alone (OA) for 24h (n = 4-5

670 cultures per condition). (C) Representative images and quantification of the density of long-

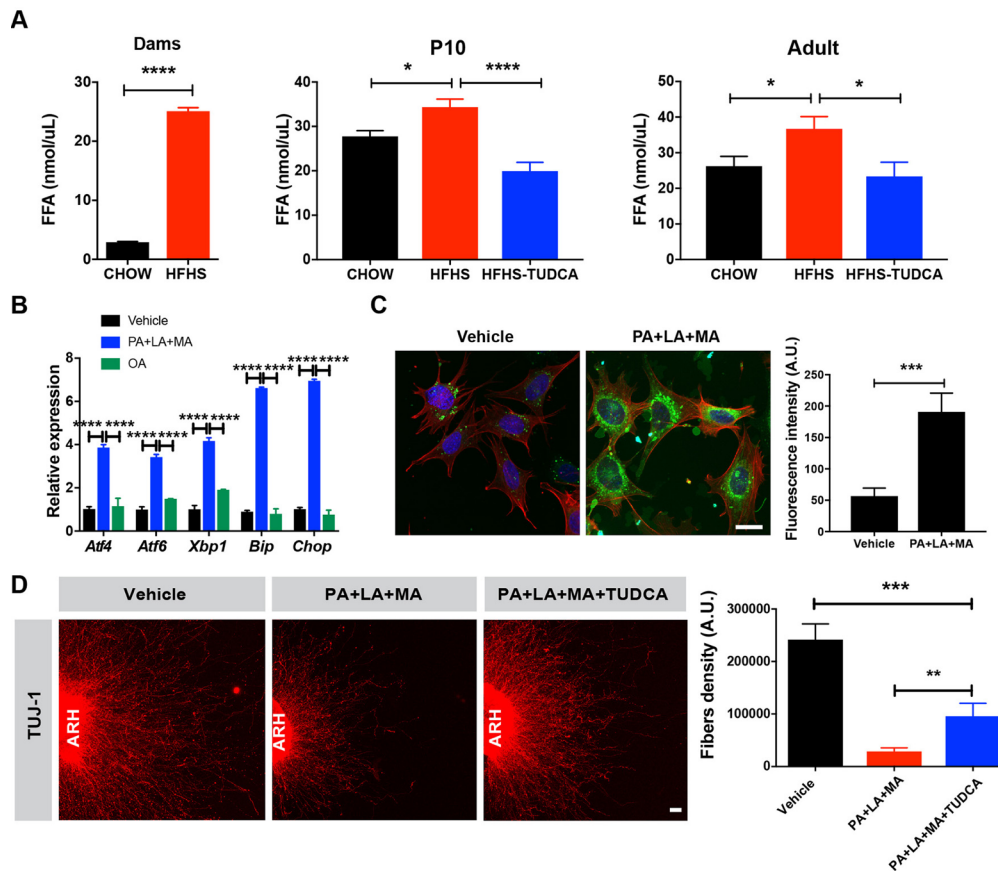
671 chain fatty acid analog BODIPY (green fluorescence) immunoreactivity in N43/5 cells treated

672 with vehicle (BSA with 0.1% ethanol) or palmitate (250  $\mu$ M) with lauric (1mM) and myristic acids

673 (200  $\mu$ M) (PA+LA+MA) for 24h (n = 5-7 cultures per condition). Red fluorescence and blue

674 fluorescence depict actin filaments phalloidin and DAPI nuclear staining, respectively. (D)

675 Confocal images and quantification of TUJ1 (neuron-specific class III beta-tubulin)



676 immunoreactive fibers derived from isolated arcuate nucleus (ARH) explants incubated with  
677 vehicle (0.1% ethanol) or a combination of palmitate (250  $\mu$ M) with lauric (1mM) and myristic  
678 acids (200  $\mu$ M) (PA+LA+MA) with or without TUDCA (750  $\mu$ g/ml, n = 6 cultures per condition).  
679 Data are presented as mean  $\pm$  SEM. \* $P$  < 0.05, \*\* $P$   $\leq$  0.01, \*\*\* $P$  < 0.001 *versus* other groups.  
680 Statistical significance was determined by unpaired two-tailed Student's t test (A, C, D), two-way  
681 ANOVA followed by Tukey's Multiple Comparison test (B). Scale bars, 20  $\mu$ m (C), and 50  $\mu$ m  
682 (D).

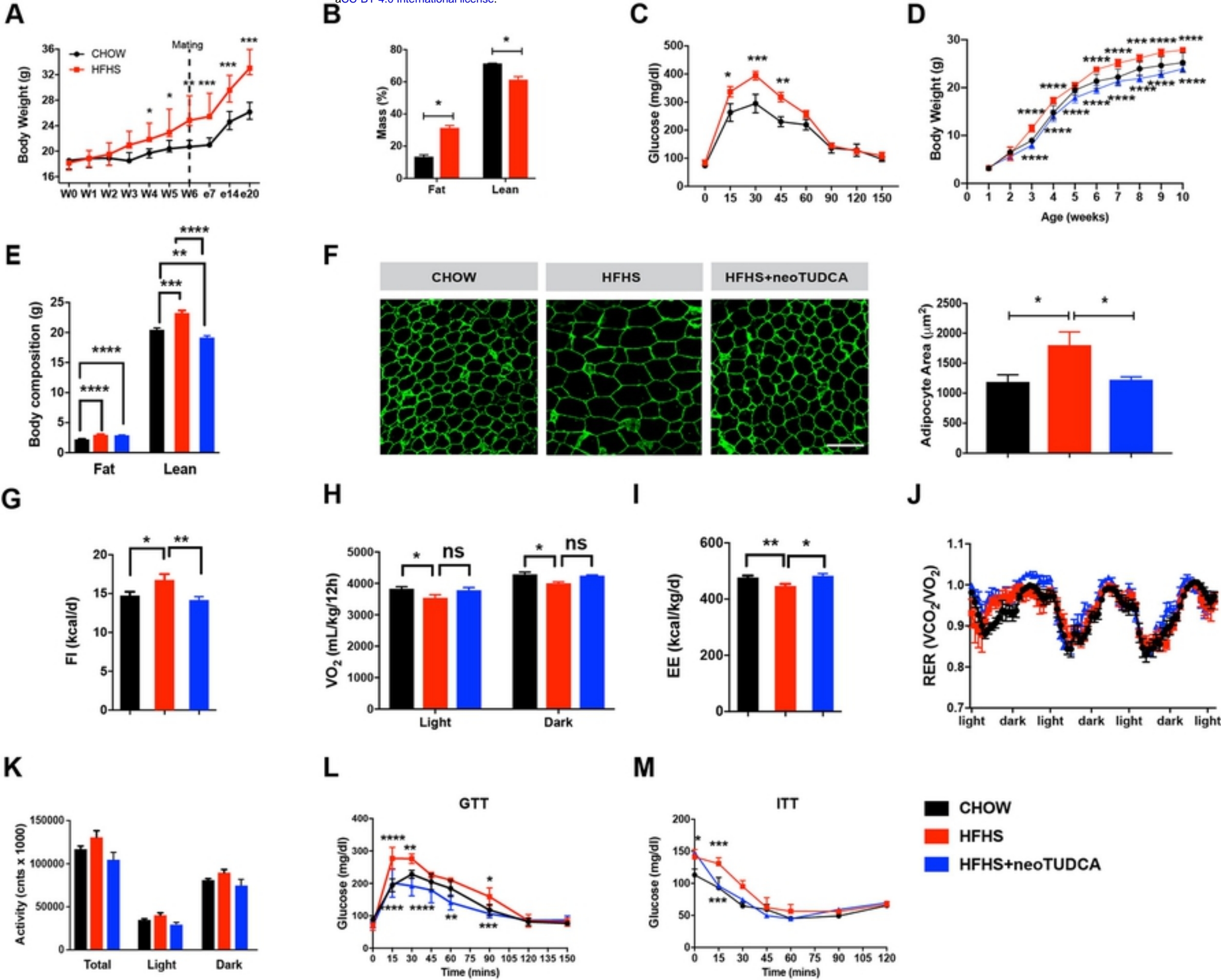


Figure 1



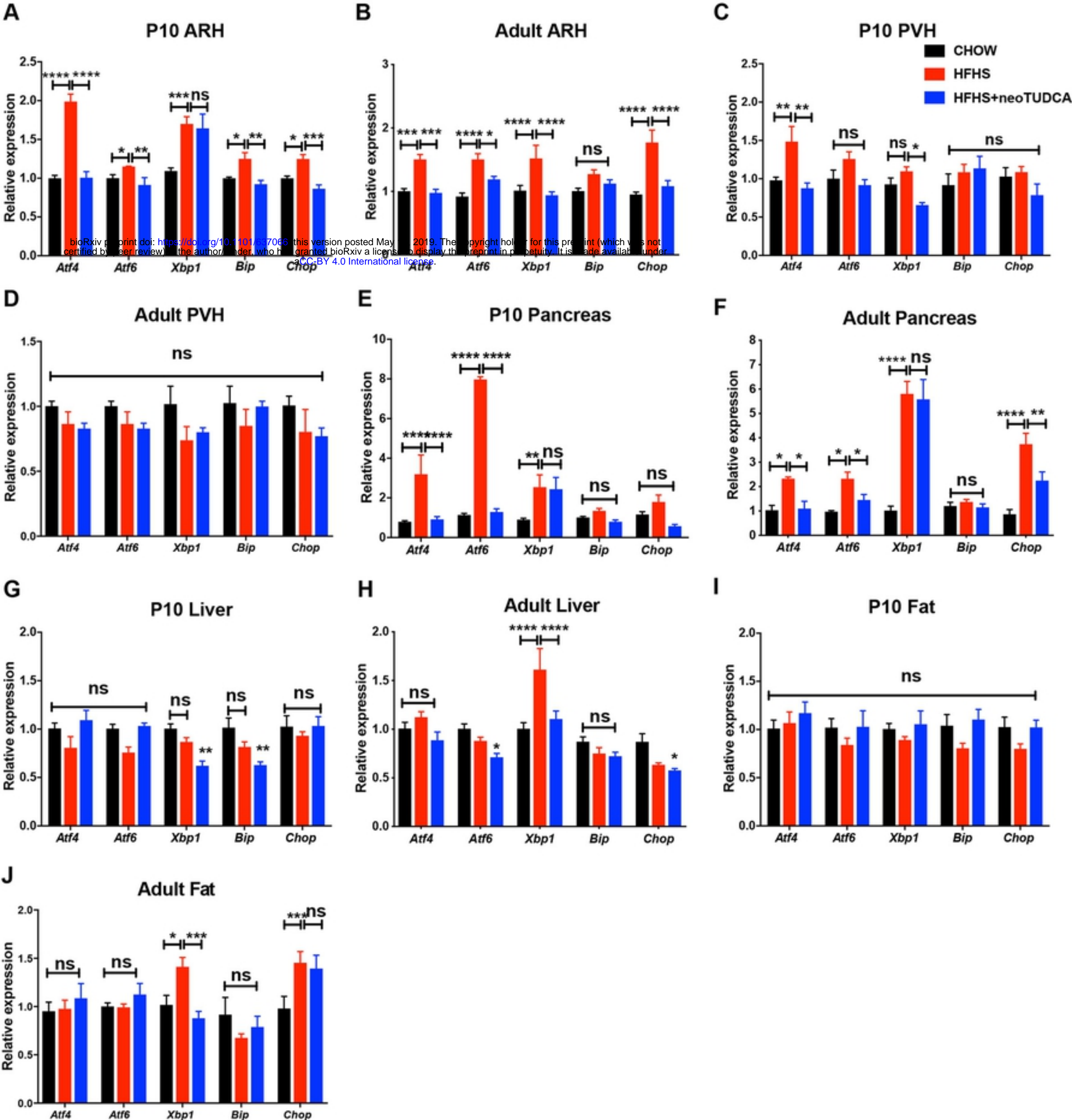


Figure 2

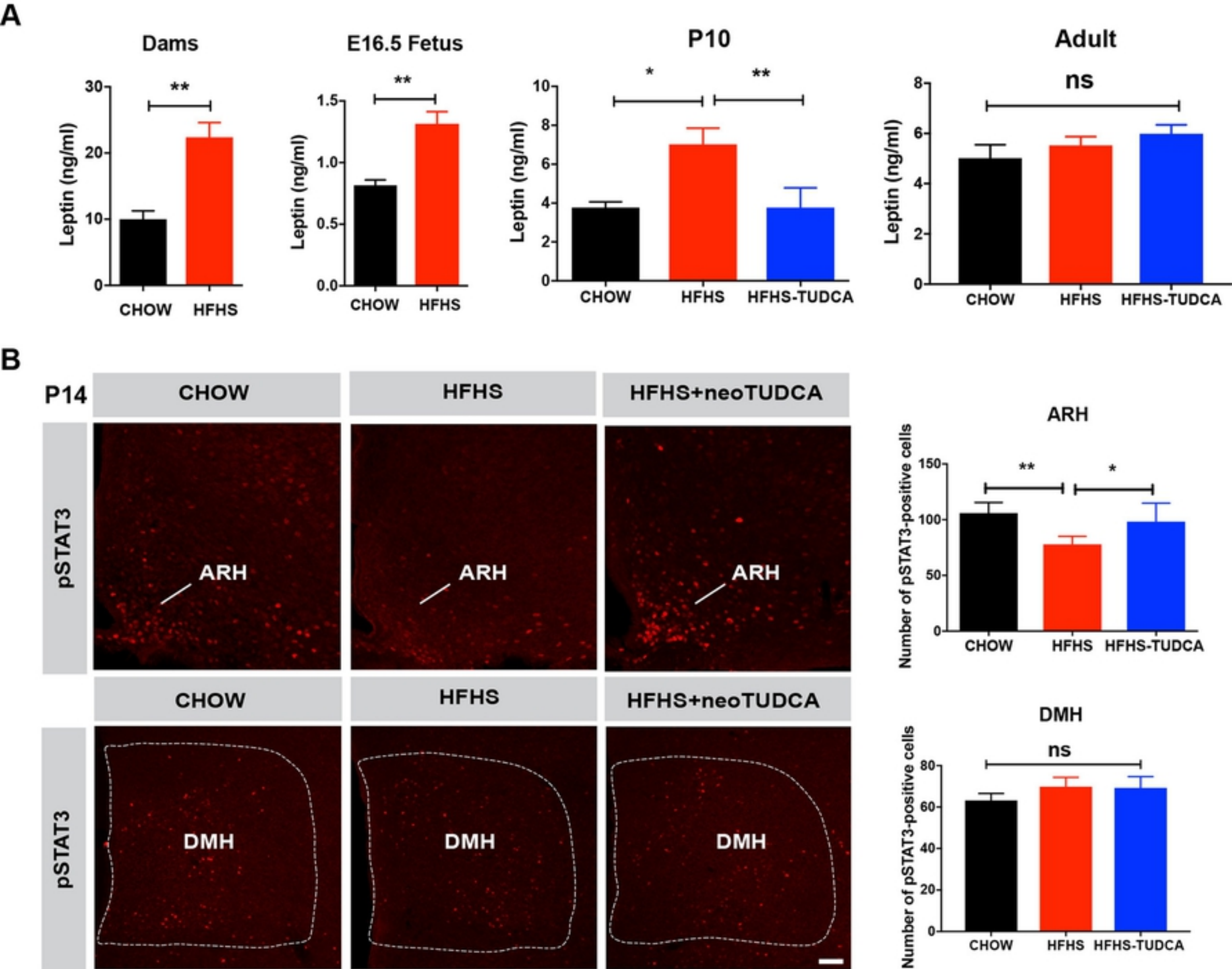


Figure 3

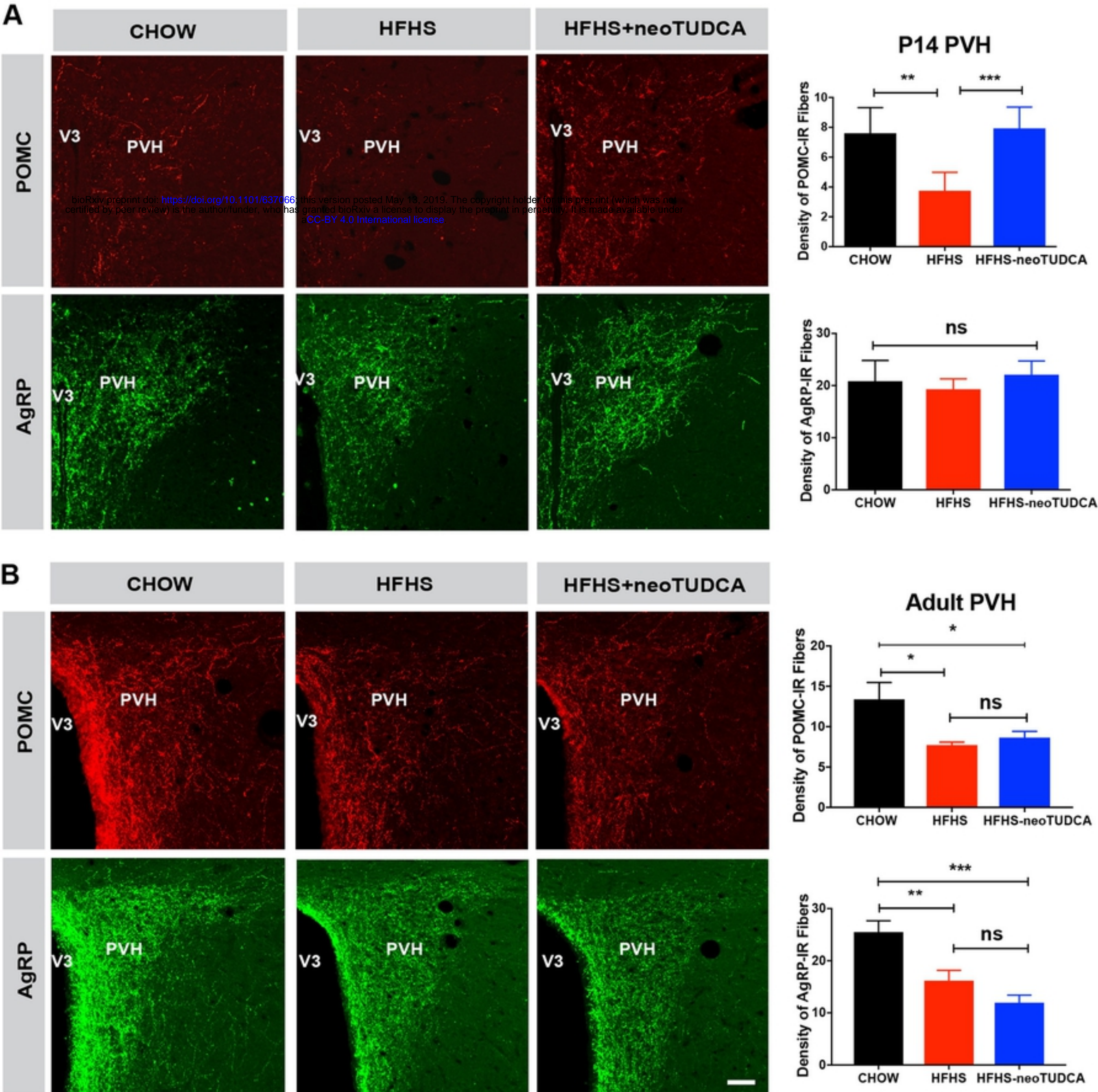


Figure 4

